

Polymer Chemistry

Accepted Manuscript



This is an *Accepted Manuscript*, which has been through the Royal Society of Chemistry peer review process and has been accepted for publication.

Accepted Manuscripts are published online shortly after acceptance, before technical editing, formatting and proof reading. Using this free service, authors can make their results available to the community, in citable form, before we publish the edited article. We will replace this *Accepted Manuscript* with the edited and formatted *Advance Article* as soon as it is available.

You can find more information about *Accepted Manuscripts* in the [Information for Authors](#).

Please note that technical editing may introduce minor changes to the text and/or graphics, which may alter content. The journal's standard [Terms & Conditions](#) and the [Ethical guidelines](#) still apply. In no event shall the Royal Society of Chemistry be held responsible for any errors or omissions in this *Accepted Manuscript* or any consequences arising from the use of any information it contains.

ARTICLE

Polyelectrolyte/Mesoporous Silica Hybrid Materials for High Performance Multiple-Detection of pH Value and Temperature

Cite this: DOI: 10.1039/x0xx00000x

Received 00th January 2015,
Accepted 00th January 2015

DOI: 10.1039/x0xx00000x

www.rsc.org/

Feng Chen^{*a,b}, Xiaoping Jiang^a, Tairong Kuang^{b,c}, Lingqian Chang^b, Dajiong Fu^{b,c}, Jintao Yang^a, Ping Fan^a and Mingqiang Zhong^{*a}

Mesoporous silica nanoparticles have been widely adopted in energy, biology and medicine due to their well-ordered and stable structures. Nevertheless, rare attempts were previously applied to study these materials as a sensing tool. We here report a “smart” sensor for dual-detection of pH value and temperature, which was implemented with environmentally responsive polyelectrolyte/mesoporous silica electrodes. Using SBA-15 silica as the framework, we functionalized the internal mesopores with DMAMEA monomer via surface-initiated RAFT polymerization (“grafting-from” method). By controlling the degree of polymerization, pore size and specific surface area can be precisely controlled. When the degree of polymerization is optimized to 75, the hybrid material showed significant sensitivity in response to pH value in the range of 4 to 10, optimally responded the temperature at 39 °C setting a pH value of 10. The ionic conductivities of template $\text{Fe}(\text{CN})_6^{4-/3-}$ and $\text{Ru}(\text{NH}_3)_6^{2+/3+}$ ions were switchable in different conditions. These results suggested that the polyelectrolyte/mesoporous silica hybrid materials could find a promising potential for the application of dual-functional sensors for environmental detection.

1 Introduction

The design, synthesis, and operation of functional interfaces with switchable properties are important in the fields of materials science and nanotechnology. For instance, bioelectricity caused by ions passing through protein ion channels on cyto-membrane is an intrinsic mechanism of nature, which exploits fixed charges in the membrane to generate differential permeabilities.¹⁻⁵ Design of biotic analogues for ion translocation through nanochannels illuminates a fascinating theme in recent years, i.e. the implementation of ionic circuits for sensing, switching and amplifying the chemical identities from aqueous environment.⁶⁻¹⁰ So far, most mechanisms of ion conduction in synthetic pores and channels are based on the notion that an “open” and “closed” state of the channel, which depends on the change of physicochemical environment across the channel.^{11,12}

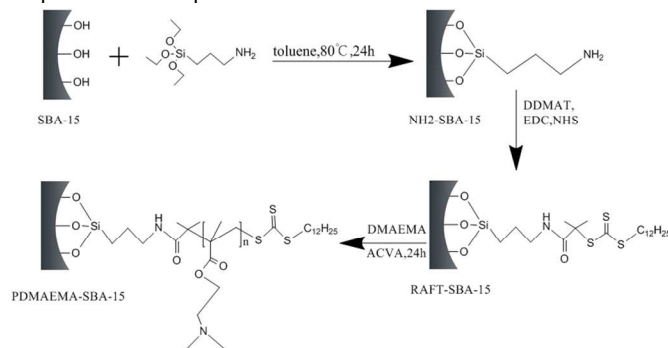
Currently, polymers are widely used in various areas due to their broad range of properties,^{13,14} and polymer-inorganic mesoporous hybrid film offers excellent platforms for realizing the biologically inspired concepts, with advanced materials and ‘active’ nanosystems.^{15,16} The versatile approach was inclined more towards ‘smart’ materials with responsive interface such as surface charge, gelatin and selective ion permselectivity.^{15,17} In these materials, mesoporous films are used as structural unit while the surface-grafted polymers as functional responsive unit.^{18,19} Thereby, the functionalization strategy, such as ‘grafting-to’ by covalent or electrostatic binding, or ‘grafting-from’ by using surface initiated polymerization methods, might result in different functional densities on planar surfaces.²⁰⁻²⁴ For mesoporous films, the incorporation of polymer brushes into the mesopores enables a better

control over the density of functional groups incorporated in the pores as well as endows the mesoporous scaffold with built-in responses to various chemical stimuli.^{11,12,16,25-29} The infiltration of polyelectrolytes into mesoporous silica, a key factor in ‘grafting-to’ approaches, has been extensively explored by Caruso and collaborators, and subsequently exploited to build up mesoporous polymer-based spheres for delivery purposes.³⁰⁻³²

Concerning ‘grafting-from’ strategies for mesoporous matrices, only few surface-initiated polymerization techniques, mainly free radical, or controlled radical polymerization, are frequently used for grafting from polymerization in mesopores.³³⁻³⁶ Although high grafting densities allow access to stimuli-responsive polymer brushes or many important applications, the characterization of polymers obtained by this method is more challenging compared to the so-called ‘grafting-to’ approach.^{17,37,38} So far polymers responsive to pH, or ionic permselectivity, were investigated as internal trigger in mesoporous silica.^{11,12,28,34,37} Specifically, poly(2-(diethylamino)ethyl methacrylate) (PDEAEMA), which has a pK_a around 7.4, has been widely used as a pH and temperature dual responsive polymer,³⁸⁻⁴⁴ and the pH and temperature critical points of PDMAEMA hydrogels are different for various systems, because they are affected by each other and other external factors.⁴² PDMAEMA can now be synthesized with an excellent control on the chemical composition and molecular weight via living radical polymerization techniques such as atom transfer radical polymerization (ATRP)^{43,44} and reversible addition-fragmentation chain transfer (RAFT) polymerization.^{39,45,46} For several applications, PDMAEMA-based materials were explored such as the

creation of a hydrophobic/hydrophilic surface,⁴⁷ for the complexation with DNA,⁴⁸ and in pH responsive micellar systems for drug encapsulation and release.⁴⁹ Nevertheless, it is still a challenge to find facile methods for fabrication of biocompatible, high environmental resistance, and highly efficient materials with dual-responsive properties. Furthermore, it is essential for fabricating nano-scale polymeric layers in such restricted mesopores (< 10 nm), to understanding the relationship between functionalized mesopores and responsive sensibility.

Here, we report the functionalization of an ordered mesoporous silica film with pH and temperature dual responsive PDMAEMA. Our strategy started from the grafting of RAFT initiator, 2-(dodecyl thiocarbonothioylthio)-2-methyl propionic acid (DDMAT) by utilizing the hydroxyl groups on the interface. Surface-initiated reversible addition-fragmentation chain transfer (SI-RAFT) polymerization was carried out to graft the double-stimuli responsive polymer, PDMAEMA, from the mesoporous silica surface, as illustrated in Scheme 1. Both methods and polymers were compared in terms of functionalization and ionic permselectivity, and a clear influence of the functionalization strategy on ionic permselectivity was observed. By taking advantage of the responses of the PDMAEMA to environmental stimuli, the pore features can be well-defined by stretching and recoiling of the PDMAEMA brushes because of their adjustable chain conformations in response to temperature and/or pH value.



Scheme 1. The synthesis process of the PDMAEMA-functionalized mesoporous silica.

2 Materials and Methods

2.1 Materials

(3-Aminopropyl)triethoxysilane (APTES), 4,4'-azobis(4-cyanovaleric acid) (ACVA), hexaammine ruthenium (II/III) chloride, potassium ferricyanide, potassium hexacyanoferrate (II), n-pentane were purchased from Aladdin Co. China. N-ethyl-N'-(3-dimethyl aminopropyl)carbodiimide hydrochloride (EDC), N-hydroxy succinimide (NHS), 2-(dimethyl amino)ethyl methacrylate (DMAEMA) were purchased from Sigma Aldrich, USA. N,N'-dimethyl formamide (DMF), chloropotassium (KCl), sodium hydroxide (NaOH), hydrochloric acid (HCl, 37% aqueous solution), hydrofluoric acid (HF, 10% aqueous solution), toluene and absolute ethanol were purchased from Sinopharm Chemical Reagent Co. China. Mesoporous silica (SBA-15, the average pore diameter is 8 nm) was purchased from XFNANO Materials Tech Co., china. 2-(Dodecyl thiocarbonothioylthio)-2-methyl propionic acid (DDMAT) was carried out as reported in the literatures.^{50,51} All other materials were used as received unless the DMAEMA monomer was distilled at reduced pressure, to remove the inhibitor. Deionized water was taken from a Milli-Q purification system.

2.2 Synthetic procedure

Synthesis of NH₂-functionalized SBA-15

The amine functionalized SBA-15 was prepared similar to the method described in the literatures.^{52,53} To a suspension of SBA-15 (3 g) in 30 mL of dry toluene, APTES (12 mL) was dissolved in 30 mL dry toluene was added dropwise, after stirring for 30 min at ambient temperature, refluxed 24 h at oil bath in 80 °C. Until the completion of reaction, the mixture was filtered, rinsed with toluene and n-pentane repeatedly, air-dried at 50 °C overnight, and then white powder (NH₂-SBA-15) was obtained.

Synthesis of RAFT-functionalized SBA-15

The NH₂-SBA-15 (2 g) was dispersed into water (30 mL) under ultrasonic and the pH value was adjusted to 5. After 20 min, EDC (0.88 g) and NHS (0.53 g) mixed with DDMAT/DMSO were dissolved in above aqueous solution and stirred at ambient temperature for half hours. Finally, the mixture was stirred vigorously at 30 °C for 24 h. Then the solid products were separated by centrifugation at 4500 rpm for 15 min was washed sequentially by methanol and deionized water. This resulting material is referred to as RAFT-SBA-15.

Modification of RAFT-SBA-15 with PDMAEMA

ACVA (0.0023 g) and RAFT-SBA-15 (0.2 g) (the molar ratio ACVA to DDMAT is 1/5) dissolved in ethanol. After ultrasonic dispersing for 0.5 h, DMAEMA (set various degree of polymerization (DP_n) with 25, 50, 75 and 100) was added to the mixture, following a vigorous stir at 70 °C for 24 h and degassing with nitrogen for 1 h at room temperature. The mixture stopped by quenching in ice water and was washed several times with ethanol to remove the residue. Finally, the obtained yellow powder (PDMAEMA-SBA-15) was dried at 60 °C overnight and for further use.

2.3 Characterizations

Transmission electron microscopy (TEM) images were recorded on a CM 200FEG transmission electron microscope operated at 200 keV. **Fourier transform infrared spectroscopy (FTIR)** spectra were acquired at room temperature using a Nicolet 6700 spectrometer with a resolution of 4 cm⁻¹ and scanning range from 4000 to 400 cm⁻¹. **Thermogravimetric analysis (TG)** was performed using SDTQ600 (TA, USA) and experiments were carried out under dry nitrogen purge at flow rate of 10 mL/min from room temperature to 800 °C at 10 °C/min. **N₂ adsorption/desorption isotherms** was carried out on a ASAT 2020M+ Apparatus, from which the BET surface area, the pore volume, and the pore size distributions were obtained based on the BJH model. **Small-angle X-ray diffraction (SAXD)** measurements were recorded on a RigakuD/MAX-2550 diffractometer, using Cu K α radiation ($\lambda=1.54\text{\AA}$). **Gel Permeation Chromatography (GPC)** measurements were performed on Waters 1525 with a differential refractive index (RI) detector at 85 °C. Styragel HR 1 and HR 4 were tandem for high-resolution columns, in a weight range of 100-600,000. DMF was used as eluent and a flow rate of 1 mL min⁻¹, adding 0.05 M LiBr for eliminating the hydrogen bond. Molecular weight and molecularweight distribution of the samples were calibrated with poly(methyl methacrylate) standards. To prepare GPC samples, the PDMAEMA-SBA-15 hybrid materials were dissolved in ethanol/HF (90/10) solution, and then the polymers were precipitated and separated. An RST4800 (Suzhou RST Co. China) electrochemical work station was used for all electrochemical measurements.⁵⁴ **Electrochemical impedance spectroscopy (EIS)** and **Cyclic Voltammetry (CV)** was conducted in 100 mM KCl solution as supporting electrolyte, the Fe(CN)₆^{4-/3-} or Ru(NH₃)₆^{2+/3+} as redox probe diffusing across the mesoporous film to studied quantitative variations in ion permselectivity following the change of

electrical signals. The pH value was adjusted with NaOH or HCl solution. The measured electrode area was 2 cm². Three-electrode cell system was used and SCE (Hg/Hg₂Cl₂) as the reference, platinum plate as the counter, the carbon electrode casted by various mesoporous silica films with the same quality as the working electrode, respectively.

3 Results and discussion

3.1 Morphological and structural characterization of hybrid materials

As described in the synthetic procedure, the modification strategy of SBA-15 involves three key steps (shown in Scheme 1). The surface hydroxyl groups were first reacted with the ethoxy groups of APTES, after then the amino groups were reacted with carboxyl groups in DDMAT to anchor RAFT agent on the NH₂-SBA-15 wall surface. Finally, DMAEMA monomer was reacted with modified SBA-15 materials.

The FTIR spectra are employed to verifying the presence of chemical groups in SBA-15, NH₂-SBA-15, RAFT-SBA-15 and PDMAEMA-SBA-15 samples. The respective FTIR curves were presented in Figure 1. FTIR spectrum of pure mesoporous silica revealed at around 3430cm⁻¹ corresponding to the O-H stretching bands of surface silanols bonds, the typical asymmetric vibration peak Si-O-Si 1085 cm⁻¹, 804 cm⁻¹ and Si-OH vibration at 972 cm⁻¹ are noted. Amino-modification of SBA-15 is confirmed by absorption peak 1560 cm⁻¹ of NH₂ on the surface of SBA-15 (Figure 1b). What is more, peaks for silanols disappear indicating the attachment of APTES to the mesoporous silica surface successfully. In addition, the appearance of a absorption new peak in case of RAFT-SBA-15 at 2925 cm⁻¹, 2850 cm⁻¹ as the presence of -CH₃ and -CH₂, 1650 cm⁻¹ are related to C=O groups⁵⁵ that implies the existence of RAFT agent of mesoporous silica surface. Ester C=O absorption peak 1730 cm⁻¹ and the intensities of -CH₃ and -CH₂ vibration at 2925 cm⁻¹, 2850 cm⁻¹ increase considerably and further indicate the immobilization of DEAEMA on mesoporous silica materials surface.

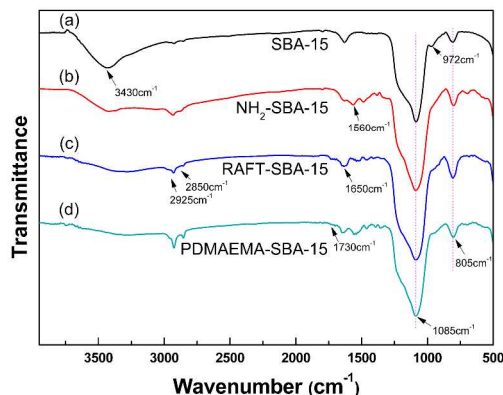


Figure 1. FTIR spectra of SBA-15 (a), NH₂-SBA-15(b), RAFT-SBA-15 (c) and PDMAEMA -SBA-15 (d).

TEM images of SBA-15 and PDEAEMA functionalized SBA-15 are presented in Figure 1. Noticeably, SBA-15 (Figure 2a and b) have parallel pore wall, uniform pore size and average diameter of about 8 nm. In contrast, the parallel stripes or arcs in PDEAEMA functionalized SBA-15 indicate that polymerization of DEAEMA do not destroy the mesoporous structure of the nanoparticles. Meanwhile, the exterior surface of the silica nanoparticles was obviously coarser, as shown in Figure 2c and d. To some extent, it also suggests that the PDEAEMA successfully grafted to the inner porewall of SBA-15 mesoporous nanoparticles.

N₂ adsorption/desorption isotherms with the corresponding pore-size distribution of the mesoporous hybrid materials are shown in Figure 3. Nitrogen adsorption/desorption isotherms for all samples show type IV pattern according to the IUPAC classification, with well-defined capillary condensation step and exhibit obvious H1 hysteresis loops in the partial pressure range of 0.4 to 0.8, which are attributed to the presence of mesopores in the obtained functionalized SBA-15. So it is confirmed that the modification of SBA-15 successively with APTES, DDMAT and DMAEMA can still retained the original hexagonal mesoporous structure of this material. Structural properties of the various mesoporous samples, calculated from the adsorption/desorption isotherm by using the Barrett-Joyner-Halenda (BJH) method, are summarized in Table 1. All samples show good uniformity, with narrow pore size distribution from 7.86 to 4.62 nm. The decreases in the pore size values, surface area and pore volume also demonstrate the successful immobilization of all organic groups in the mesopores channel of the SBA-15.

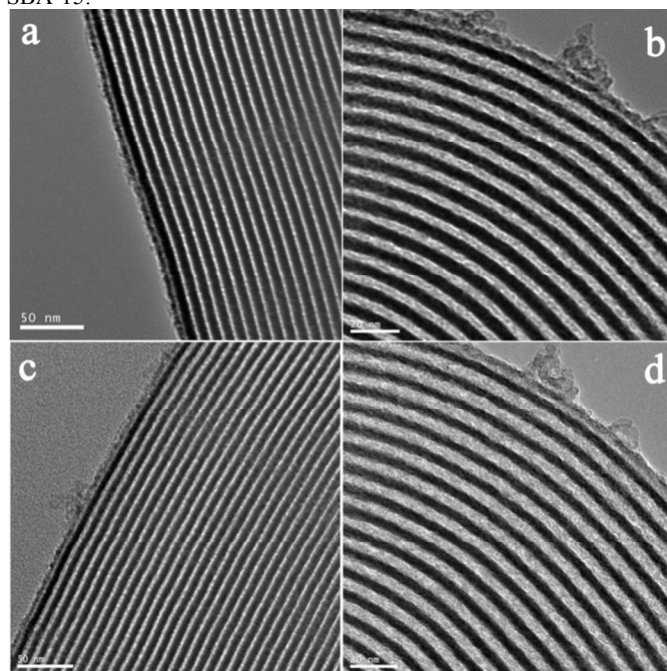


Figure 2. TEM images of the SBA-15 (a and b) and PDEAEMA functionalized SBA-15 (c and d). scale bar: a & c, 50 nm; b & d, 20 nm.

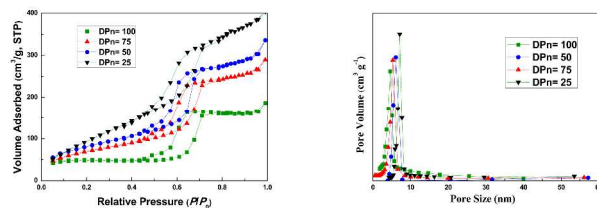


Figure 3. Adsorption/desorption isotherm and pore size distribution curves for various PDMAEMA-modified mesoporous silica.

Table 1. Structural properties of mesoporous hybrid materials and the SBA-15 support characterized by N₂ adsorption/desorption analysis.

DPn	Average Pore Diameter (nm)	Surface Area (m ² /g)	Pore Volume (cm ³ /g)
0	7.86	513.10	0.87
25	7.13	403.17	0.63
50	6.11	297.60	0.52

75	5.34	242.94	0.45
100	4.62	182.45	0.29

Figure 4 shows the powder X-ray diffraction patterns in different DPn values (25, 50, 75 and 100, respectively). Three reflection peaks of samples ($2\theta=1.0^\circ$, 1.7° and 2.0°), are attributed to (100), (110), and (200) porewall orientation, respectively, indicating that the good mesoscopic order and two-dimensional hexagonal structures of SBA-15 are maintained after RAFT polymerization, compared to the parent SBA-15 support. Moreover, from the XRD patterns SBA-15, with or without modification, strong decrease peak intensity is observed with the increase of DPn as compared to SBA-15 materials, this means that the mesopores ordering decreased with reacted with other organic groups. The peak pattern, however, remains intact, illustrating the grafting of the organic occurs mainly inside the mesopores channels.

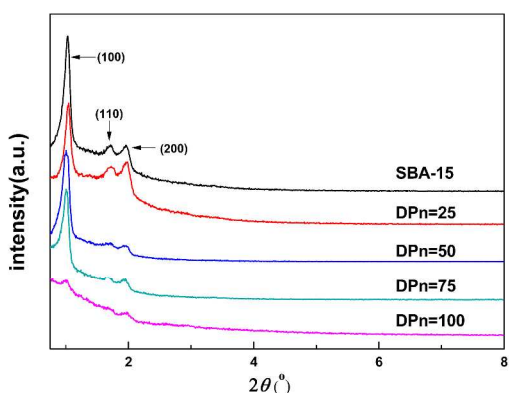


Figure 4. XRD patterns of mesoporous hybrid materials and the SBA-15 support.

Thermogravimetric analysis of the functionalized mesoporous silica was conducted from 20 to 800 °C under nitrogen and TG profiles shown in Figure 5. The pure mesoporous silica SBA-15 has 7.98% weight loss at temperature of to 800 °C, attributed to the loss of surface decomposition of silanols groups and small amount of adsorbed water. In the case of NH_2 -SBA-15 and RAFT-SBA-15, the weight loss is 13.06 and 16.57 wt%, respectively, due to the decomposition of little functionalized organic matter (base APTES and DDMAT). Since the DMAEMA is grafted onto the surface of the mesoporous materials, the weight loss rises sharply to 30.18% (sample with 100 DPn). The phenomenon implies that the DMAEMA monomers have the polymerization reaction successfully again.

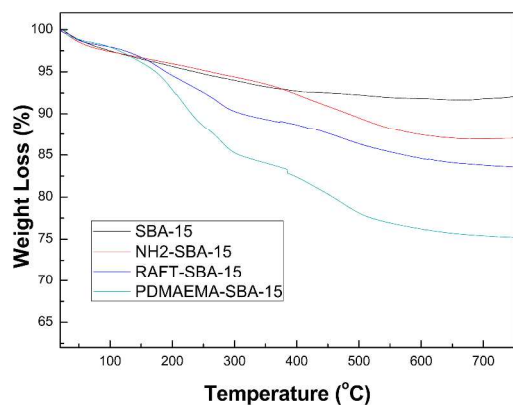


Figure 5. TGA curves of SBA-15, NH_2 -SBA-15, RAFT-SBA-15 and PDMAEMA-SBA-15 (100 DPn) samples.

GPC analysis of functionalized SBA-15 products with different DPn shown in figure 6 and the analysis results for all materials are shown in Table 2 along with the polydispersity (PDI). As shown in Figure 6 and Table 2, the grafted polymers have approximate molecular weight with theory DPn of 25, 50, 75 and 100. Meanwhile, PDMAEMA have a very narrow molecular weight distribution more than 1.16, which follow the unique law of RAFT polymerization. In a conclusion, the RAFT polymerization can be successfully surface-initiated from the porewall of mesoporous silica. As a result, the PDMAEMA-grafted mesoporous silica composites were synthesized. The pore size was easily adjusted as the DPn of grafted polymer was exactly controlled. Particularly, it is very interesting in the relationship between the thickness of graft polymer and electrochemical property.

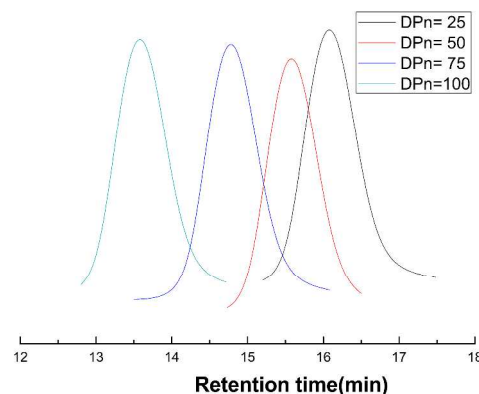


Figure 6. GPC traces of PDMAEMA brushes separated from various mesoporous hybrid materials.

Table 2. GPC characterization results of PDMAEMA brushes at different degree of polymerization (DPn).

DPn	M_n (theory)	M_n (GPC)	M_w/M_n (PDI)	Retention Time (min)
25	3930	4020	1.06	16.3
50	7861	8000	1.12	15.5
75	11791	11300	1.11	14.8
100	17686	16000	1.10	13.5

3.2. Electrochemical measurement

Observing the PDMAEMA polymer is sensitive to pH and thermal change, we fabricated a sensor by drop-coating the mesoporous silica composites film on a carbon electrode, with the protocol showed in the literature.^{56,57} The sensor was characterized using electrochemical impedance spectroscopy (EIS) in a 100mM KCl solution. The EIS measured through three-electrode cell system⁵⁸ to obtained mesoporous films bulk resistance (R_b), which can calculate the ionic conductivity through the mesoporous channels following the equations:

$$\gamma = \frac{1}{R_b} \times \frac{D}{S}$$

Where γ is the mesoporous films ionic conductivity, R_b is the mesoporous film's bulk resistance, D is the thickness of carbon working electrode, and S is the area of coated modified mesoporous films.

Figure 7a showed that the ionic conductivity of the produced sensor significantly dropped with the increase of pH, in the range of 4 to 10. At DPn 25, no obvious sensitivity was observed, which might result from the few polymers grafted on the inner wall of the pores where ions move freely. When DPn increases to 50, mesoporous film just have slightly responsiveness. Particularly,

when DPn reaches 75, mesoporous film exhibited significantly sensitive and ionic conductivity alter rapidly between 7 and 8, which in accord with previous reported (PDMAEMA $pK_a = 7.4$),^{41,48} reflecting the controllability to pH of the mesoporous film in some way. However, at DPn 100, the excess grafting polymer inner wall mesoporous caused film pore blocking and ions cannot through smoothly. This is can explain that why ionic conductivity remaining constant at DPn 100.

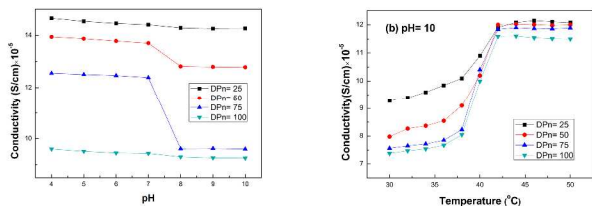


Figure 7. The ionic conductivity of mesoporous hybrid materials (a) as a function of pH at room temperature and (b) as a function of temperature at pH 10.

It is well-known that the environmental response of the PDMAEMA is a typical LCST behaviour; the variation on the PDMAEMA chain conformation is strongly dependent upon temperature and the corresponding pH value in aqueous solution; for example, the LCST at pH 2 is above 85 °C, at pH 7 is around 65 °C, and is below 35 °C, once the pH raises to 11.^{59,60} At low pH, PDMAEMA can be protonated and ionized in aqueous solution with grafted polymer swelling perfectly show the strong hydrophilicity, and no LCST is detected under 50 °C. That is the consequence of hydrophobic (dedicated to the isopropyl groups) and hydrophilic (dedicated to the tertiary amine groups). As increasing pH, the swelling ratio decreases rapidly will shift towards a little hydrophilic nature. Until pH 8, polymer chains intertwining and congregating inside pore wall of mesoporous silica gradually show the LCST at the macro level. When $pH \geq 10$, polymer chains aggregation completely. In these conditions, mesoporous response films relates exclusively to temperature, and not to pH. Former work in Müller's group compared the LCST behaviour of linear and star-shaped PDMAEMA depending on molecular weight, concentration, and pH.^{59,60} In biological channels, the mainly biochemical reactions are triggered between 30 to 50 °C. Here, the LCST for a graft PDMAEMA with a DPn 100 was determined 39 °C at pH 10. Therefore, we choose the typical point pH 10 to investigating the changed of mesoporous film's ionic conductivity following R_b .

As presented in Figure 7b, it is obvious that ionic conductivity shifts suddenly around 40 °C under the specified conditions to demonstrate clearly the temperature responsive of functionalized mesoporous films. When increased DPn from 25 to 100, the LCST decreased slightly from 40 to 39 °C. It is attributed to the effect of total deprotonation, resulting in the recoil of the examined PDMAEMA brushes; consequently, this provides the obviously increment of the ionic conductivity. For the case reported here, no difference could be seen between the phase transition temperatures (LCST) compared to linear PDMAEMA homopolymer. Note that the situation for a polymer brush confined on the pore surface. These results inspired us to use the mesoporous films to control the electrochemical switchable property by switching solution pH or temperature.

To investigate the ionic transport properties of the hybrid interfacial assemblies, the diffusion of charged species through mesoporous films supported on electrode was electrochemically probed by CV using $Fe(CN)_6^{4-/3-}$ as an anionic redox probe and $Ru(NH_3)_6^{2+/3+}$ as a cationic redox probe, respectively. The proton concentration acts as an accurate chemical parameter responsible for setting different electrostatic conditions in the pore. As is well-known, the emergence

of permselectivity effects or ionic gating requires the presence of surface charges on the mesopore walls. At $pH < pK_a$ the dominant species in the brush are fully protonated DMAEMA ammonium salt.

Figure 8 comparatively displays the CV curves of PDMAEMA-grafted (DPn=75) SBA-15 hybrid electrode in the presence of 1 mM $Ru(NH_3)_6^{3+}$ (Figure 8a and b) and $Fe(CN)_6^{3-}$ (Figure 8c and d) as the supporting electrolyte. The electrochemical data reveals that the fully protonated pore behaves as an open gate enabling the free diffusion of anionic and cationic species through the film. Changes in the voltammetric response of mesoporous electrodes reflect the changes in probe concentration or diffusion due to the architecture or electrostatic environment of the pores. It is observed that increasing pH above pK_a (7.4) has a significant effect on the transport properties of the mesoporous film. In a 30 °C solution, the electrochemical current of $Fe(CN)_6^{3-}$ decreased from 37 to 11 $\mu A/cm^2$, whereas the current of $Ru(NH_3)_6^{3+}$ increased from 15 to 138 $\mu A/cm^2$. The generation of DMAEMA anionic units in the mesoporous films enhanced the voltammetric signal of $Ru(NH_3)_6^{3+}$ ions dissolved in the electrolyte solution. Hence, increasing pH from 4 to 10 increased the ratio of electrochemical currents of cationic (I_{Ru}) and anionic (I_{Fe}) redox probes from 0.4 to 12.5 as a result of the combination of permselective exclusion of anionic probes and preconcentration of cationic probes.^{11,12,28}

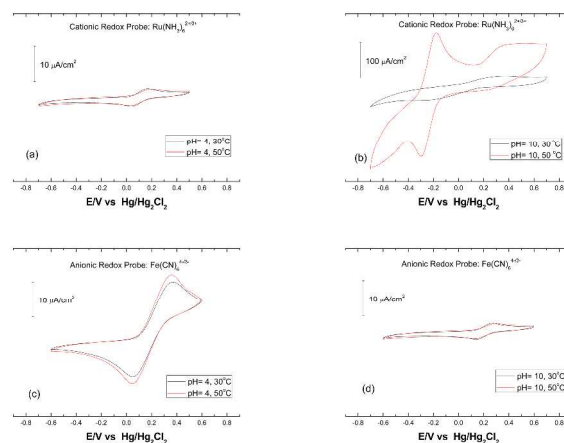


Figure 8. Comparative cyclic voltammograms displaying the molecular transport through PDMAEMA-functionalized mesoporous thin films as functions of pH and temperature using (a-b) $Ru(NH_3)_6^{2+/3+}$ as a cationic redox probe and (c-d) $Fe(CN)_6^{4-/3-}$ as an anionic redox probe. Scan rate: 200 mV/s. Electrolyte: 1 mM redox probe + 100mMKCl under different pH conditions (pH 4 and pH 10) and temperature conditions (30 °C and 50 °C). The DPn of PDMAEMA brush is selected as 75.

As expected, further increasing temperature above LCST (39 °C) evidenced a more pronounced gating response of the interfacial assembly because PDMAEMA brushes were fully deprotonated, and the freely mobile expanded chains collapse inside the pores. At pH=10 in a 50 °C solution, a well-defined electrochemical response of $Ru(NH_3)_6^{3+}$ ions was observed (172 $\mu A/cm^2$), whereas similar experiments performed in the presence of $Fe(CN)_6^{3-}$ revealed that the electron transfer at the underlying mesoporous film was strongly hindered (14 $\mu A/cm^2$). This can be ascribed to the fact that the fully charged anionic DMAEMA units completely exclude the anionic probes from the inner surroundings of the inorganic film. As an outcome of the interplay between preconcentration and exclusion effects, thus revealing that the pH induced generation of charges in the mesopores plays a critical role in the modulation of the gating properties, and the temperature-induced gelation can consolidate this "gate" switchable state. Due to the higher LCST of PDMAEMA at

pH < 8, the PDMAEMA chains have no phase separation behaviour at pH 4, when environmental temperature is mutative in the range of 30 to 50 °C; consequentially, neither cationic nor anionic probe exhibit a remarkable increment of ionic conductivity.

4 Conclusions

In summary, we successfully prepared double stimuli-responsive mesoporous silica hybrids via the SI-RAFT method from a PDMAEMA polymer. The structures exhibit well-controlled polymer molecular weight and homogeneous covering of the brushes, forming a biomimetic smart ionic channel with high potential for versatile applications. The ionic conductivity of serial PDMAEMA-grafted silica suggests that a desirable degree of polymerization is of proposition in 75. The variations on the CV profiles give clear evidence for the conformational changes of PDMAEMA driven by varying the pH and temperature. In the case of pH, the electrostatic characteristics of environments arising from the protonation state of tertiary amine groups are responsible for tuning the ionic transport of anionic and cationic redox probes across the mesoporous framework over a wide range of pH values. Increasing pH from 4 to 10 led to a significant increase in (anion) permselectivity and (cation) preconcentration, thus reflecting the ability of the PDMAEMA brush-modified mesopores to act as a selective “electrostatic nanovalve” precluding and boosting the anionic and cationic transport, respectively.⁶¹⁻⁶⁵ On the other hand, the gelation of PDMAEMA brushes above LCST (39 °C at DPn 75) also allowed the generation of gate-like hybrid ensembles. Our results demonstrate that the hybrid interface at pH 10 reversibly switches from low to high cationic conductance states depending on the totally collapsed conformation of PDMAEMA brushes in the mesopores. Hence, at high pH values, PDMAEMA-modified pores are strongly permselective precluding the transport of anionic probes. Because of the environment selective conformational behaviour, the as-designed system can give the potential for being a versatile double-stimuli-responsive nanoreactor, such as controlled release, nanoscale filter, environmental sensor, and biomimetic on/off gate.

Acknowledgements

This material is based upon work funded by Natural Science Foundation of China under Grant No. 21274131, 51273178, 51203139 and 51303158. Last but not least, all the laboratory membranes and co-workers are appreciated for the kindly discussion and assistance.

Notes and references

^a College of Materials Science and Engineering, Zhejiang University of Technology, Hangzhou 310014, China.

^b Department of Biomedical Engineering, The Ohio State University, Columbus, Ohio 43210, USA.

^c National Engineering Research Center of Novel Equipment for Polymer Processing, South China University of Technology, Guangzhou 510640, China.

* Coresponded Author: Prof. Jintao Yang (email: yangjt78@hotmail.com); Prof. Mingqiang Zhong (email: zhongmq@zjut.edu.cn)

- 1 B. Hille, Ion Channels of Excitable Membranes, Sinauer Associates, Sunderland, 2001.
- 2 C. Dekker, *Nature Nanotechnology*, 2007, 2, 209-215
- 3 X. Hou, W. Guo and L. Jiang, *Chemical Society reviews*, 2011, 40, 2385-2401.

- 4 X. Hou, H. Zhang and L. Jiang, *Angewandte Chemie*, 2012, 51, 5296-5307.
- 5 W. Guo, Y. Tian and L. Jiang, *Accounts of Chemical Research*, 2013, 46, 2834-2846.
- 6 W. Sparreboom, A. van den Berg and J. C. T. Eijkel, *Nature Nanotechnology*, 2009, 4, 713-720.
- 7 P. E. Boukany, A. Morss, W. C. Liao, B. Henslee, H. C. Jung, X.L. Zhang, B. Yu, X. M. Wang, Y. Wu, L. Li, K. L. Gao, X. Hu, X. Zhao, O. Hemminger, W. Lu, G. P. Lafyatis and L. J. Lee, *Nature Nanotechnology*, 2011, 6, 747-75
- 8 J. Gao, W. Guo, D. Feng, H. Wang, D. Zhao and L. Jiang, *Journal of the American Chemical Society*, 2014, 136, 12265-12272.
- 9 W. Guo, C. Cheng, Y. Wu, Y. Jiang, J. Gao, D. Li and L. Jiang, *Advanced Materials*, 2013, 25, 6064-6068.
- 10 Z. Dai and H. Ju, *TrAC Trends in Analytical Chemistry*, 2012, 39, 149-162.
- 11 B. Yameen, M. Ali, R. Neumann, W. Ensinger, W. Knoll and O. Azzaroni, *Journal of the American Chemical Society*, 2009, 131, 2070-2071.
- 12 A. Brunsen, C. Diaz, L. I. Pietrasanta, B. Yameen, M. Ceolin, G. J. Soler-Illia and O. Azzaroni, *Langmuir*, 2012, 28, 3583-3592.
- 13 E. N. Savariar, K. Krishnamoorthy and S. Thayumanavan, *Nature Nanotechnology*, 2008, 3, 112-117.
- 14 J. Song, J. Xie, C. Li, J. H. Lu, Q. F. Meng, Z. Yang, R. J. Lee, D. Wang and L. S. Teng, *International journal of pharmaceuticals*, 2014, 472, 296-303.
- 15 G. J. Soler-Illia and O. Azzaroni, *Chemical Society reviews*, 2011, 40, 1107-1150.
- 16 J. Elbert, F. Krohm, C. Rüttiger, S. Kienle, H. Didzoleit, B. N. Balzer, T. Hugel, B. Stühn, M. Gallei and A. Brunsen, *Advanced Functional Materials*, 2014, 24, 1591-1601.
- 17 R. Barbey, L. Lavanant, D. Paripovic, N. Schüwer, C. Sugnaux, S. Tugulu, and H. A. Klok, *Chemical Reviews*, 2009, 109, 5437-5527.
- 18 Q. Zhao, J. Dunlop, X. Qiu, F. Huang, Z. Zhang, J. Heyda, J. Dzubiella, M. Antonietti and J. Yuan, *Nature Communications*, 2014, 5, 5293-5300.
- 19 Q. Zhao, M. Yin, A. P. Zhang, S. Prescher, M. Antonietti, and J. Yuan, *Journal of the American Chemical Society*, 2013, 135, 5549-5552.
- 20 F. Krohm, H. Didzoleit, M. Schulze, C. Dietz, R. W. Stark, C. Hess, B. Stuhn and A. Brunsen, *Langmuir*, 2014, 30, 369-379.
- 21 G. Graffius, F. Bernardoni and A. Y. Fadeev, *Langmuir*, 2014, 30, 14797-14807.
- 22 J. F. Gnichwitz, R. Marczak, F. Werner, N. Lang, N. Jux, D. M. Guldi, Wolfgang and A. H. Peukert, *Journal of the American Chemical Society*, 2010, 132, 17910-17920
- 23 J. Yang, Y. Sang, F. Chen, Z. Fei and M. Zhong, *The Journal of Supercritical Fluids*, 2012, 62, 197-203.
- 24 P. Xie, P. He, Y.-C. Yen, K. J. Kwak, D. Gallego-Perez, L. Chang, W.-c. Liao, A. Yi and L. J. Lee, *Surface and Coatings Technology*, 2014, 258, 174-180.
- 25 B. V. V. S. P. Kumar, K. V. Rao, S. Sampath, S. J. George and M. Eswaramoorthy, *Angewandte Chemie-International Edition*, 2014, 53, 13073 -13077.
- 26 M. Bouchoucha, R. C.-Gaudreault, M.-A. Fortin and F. Kleitz, *Advanced Functional Materials*, 2014, 24, 5911-5923.
- 27 A. Brunsen, J. Cui, M. Ceolin, A. del Campo, G. J. Soler-Illia and O. Azzaroni, *Chemical Communications*, 2012, 48, 1422-1424.
- 28 B. Yameen, A. Kaltbeitzel, G. Glasser, A. Langner, F. Muller, U. Gosele, W. Knoll and O. Azzaroni, *ACS Applied Materials*

- And Interfaces*, 2010, 2, 279-287.
- 29 J. Wang, M.-Y. Su, J.-Q. Qi and L.-Q. Chang, *Sensors and Actuators B: Chemical*, 2009, 139, 418-424.
- 30 A. S. Angelatos, Y. Wang and F. Caruso, *Langmuir*, 2008, 24, 4224-4230.
- 31 Y. Wang, A. S. Angelatos, D. E. Dunstan and F. Caruso, *Macromolecules*, 2007, 40, 7594-7600.
- 32 Y. Wang and F. Caruso, *Chemistry of Materials*, 2006, 18, 4089-4100.
- 33 M. Sarsabili, M. Parvini, M. Salami-Kalajahi and P. Ganjeh-Anzabi, *Advances in Polymer Technology*, 2013, 32, 21372.
- 34 M. Ma, S. G. Zheng, H. R. Chen, M. H. Yao, K. Zhang, X. Q. Jia, J. Mou, H. X. Xu, R. Wu and J. L. Shi, *Journal of Materials Chemistry B*, 2014, 2, 5828-5836.
- 35 X. Mei, D. Chen, N. Li, Q. Xu, J. Ge, H. Li and J. Lu, *Microporous and Mesoporous Materials*, 2012, 152, 16-24.
- 36 Y. Yang, X. Yan, Y. Cui, Q. He, D. Li, A. Wang, J. Fei and J. Li, *Journal of Materials Chemistry*, 2008, 18, 5731-5737.
- 37 M. Save, G. Granvorka, J. Bernard, B. Charleux, C. Boissière, D. Grosso and C. Sanchez, *Macromolecular Rapid Communications*, 2006, 27, 393-398.
- 38 C. Song, W. Shi, H. Jiang, J. Tu and D. Ge, *Journal of Membrane Science*, 2011, 372, 340-345.
- 39 Y. Kotsuchibashi, M. Ebara, T. Aoyagi and R. Narain, *Polymer Chemistry*, 2012, 3, 2545-2550.
- 40 F. Schacher, T. Rudolph, F. Wieberger, M. Ulbricht and A. H. Müller, *ACS Appl Mater Interfaces*, 2009, 1, 1492-1503.
- 41 F. A. Plamper, M. Ruppel, A. Schmalz, O. Borisov, M. Ballauff and A. Müller, *Macromolecules*, 2007, 40, 8361-8366.
- 42 D. Fournier, R. Hoogenboom, H. L. T. Thijs, R. M. Paulus and U. S. Schubert, *Macromolecules*, 2007, 40, 915-920.
- 43 H.C. Lee, H.Y. Hsueh, U. S. Jeng and R.M. Ho, *Macromolecules*, 2014, 47, 3041-3051.
- 44 S. Ma, J. Liu, Q. Ye, D. Wang, Y. Liang and F. Zhou, *Journal of Materials Chemistry A*, 2014, 2, 8804.
- 45 F. Chen, D. X. Dai, J. T. Yang, Z. D. Fei and M. Q. Zhong, *Journal of Macromolecular Science, Part A: Pure and Applied Chemistry*, 2013, 50, 1002-1006.
- 46 Q. Li, X. He, Y. Cui, P. Shi, S. Li and W. Zhang, *Polymer Chemistry*, 2015, 6, 70-78.
- 47 E. Stratakis, A. Mateescu, M. Barberoglou, M. Vamvakaki, C. Fotakis and S. H. Anastasiadis, *Chemical Communications*, 2010, 46, 4136-4138.
- 48 J. F. Tan, H. P. Too, T. A. Hatton and K. C. Tam, *Langmuir*, 2006, 22, 3744-3750.
- 49 S. Yusa, M. Sugahara, T. Endo and Y. Morishima, *Langmuir*, 2009, 25, 5258-5265.
- 50 A. Isakova, P. D. Topham and A. J. Sutherland, *Macromolecules*, 2014, 47, 2561-2568.
- 51 Z. Elnaz, H. A. Vahid and R. M. Hossein, *RSC Advances*, 2014, 4, 31428-31442.
- 52 A. L. Doadrio, J. M. Sánchez-Montero, J. C. Doadrio, A. J. Salinas and M. Vallet-Regí, *Microporous and Mesoporous Materials*, 2014, 195, 43-49.
- 53 J. Yang, L. Huang, Y. Zhang, F. Chen and M. Zhong, *Journal of Applied Polymer Science*, 2013, 130, 4308-4317.
- 54 F. Chen, W. Zhou, H. Yao, P. Fan, J. Yang, Z. Fei and M. Zhong, *Green Chemistry*, 2013, 15, 3057-3063.
- 55 T. R. Kuang, H. Y. Mi, D. J. Fu, X. Jing, B. Y. Chen, W. J. Mou and X. F. Peng, *Industrial & Engineering Chemistry Research*, 2015, 54, 758-768.
- 56 S. Zhou, J. Li, F. Zhang, T. Zhang, H. Huang and W. Song, *Microporous and Mesoporous Materials*, 2015, 202, 73-79.
- 57 J. B. Raoofa, F. Chekin and V. Ehsani, *Sensors and Actuators B*, 2015, 207, 291-296.
- 58 L. Chang, C. Liu, Y. He, H. Xiao and X. Cai, *Science China Chemistry*, 2010, 54, 223-230.
- 59 F. Schacher, M. Ulbricht and A. H. E. Müller, *Advanced Functional Materials*, 2009, 19, 1040-1045.
- 60 D. Fournier, R. Hoogenboom, H. M. L. Thijs, R. M. Paulus and U. S. Schubert, *Macromolecules*, 2007, 40, 915-920.
- 61 E. H. Otal, P. C. Angelomé, S. Aldabe-Bilmes and G.J.A.A. Soler-Illia, *Advanced Materials*, 2006, 18, 934-938.
- 62 Y. Yamauchi, N. Suzuki and T. Kimura, *Chemical Communication*, 2009, 5689-5691.
- 63 M. C. Fuertes, F. J. López-Alcaraz, M. C. Marchi, H. Troiani, V. Luca, H. Míguez and G. J. A. A. Soler-Illia, *Advanced Functional Materials*, 2007, 17, 1247-1254.